European Conference on Computational Fluid Dynamics
ECCOMAS CFD 2006
P. Wesseling, E. Oñate, J. Périaux (Eds)

A COMPREHENSIVE MULTI-SCALE APPROACH FOR VAPOR-PHASE SYNTHESIS OF METAL OXIDE PARTICLES

G. Manenti, F. Di Muzio and M. Masi

Dipartimento di Chimica Materiali e Ingegneria Chimica "Giulio Natta", Politecnico di Milano,
Via Mancinelli 7, 20131 Milano, Italy
e-mail: maurizio.masi@polimi.it
Web page: **h**ttp://www.chem.polimi.it

Key words: Multi-scale, Vapor-phase synthesis, Metal oxide particles, Population balance

Abstract. *Synthesis of metal oxide nano- and micro-sized particles by chemical vapor-phase route is a technologically and commercially competitive process. Linking reactor operation parameters to the particle properties represents the most critical task in designing such processes. A multi-scale modelling approach applied to industrial and laboratory scale reactors of different complexity for different ceramic materials will be presented here. The model fully couples together the fluid dynamics equations and particle population balance ones. From a practical point of view, the model was implemented in two different commercial CFD codes and the following systems were analyzed: the growth of SiO_2 based performs and the synthesis of TiO_2 and ZrO_2 powders.*

1 INTRODUCTION

Several materials for advanced applications such as catalysis, electronics or bioengineering are produced through aerosol reactors, as they lend themselves to be designed at industrial scale. Aerosol reactors allow continuous and high production capacity, reduced environmental impact and good control of product quality[1,2]. At a large industrial scale, well-run aerosol processes are carbon black production for tyre industry, optical fibres and fumed silica for telecommunications, TiO_2 for pigments. At a smaller scale, Al_2O_3, SnO_2 and precious metals, such as Pt and Au, represent examples of size-controlled particles obtained by aerosol process to be used as ceramic micro-layers, gas sensors and electronic circuit components respectively.

The common characteristic of aerosol processes resides in stringent and high quality specifications on the final product, as geometrical dimensions of particles, chemical composition, morphological and optical properties. These quality requirements are more important for nano-particles, for which physical, optical and electric properties differ from

micro- and macro-particles. In order to meet product specifications without designing reactors by an expensive trial-and-error method, a multi-scale modelling approach is necessary: the task is to link reactor macro-scale parameters, as operating conditions and geometry, to the physical-chemical phenomena occurring at particle scale, by which as-synthesised particle distribution function (PDF) and their main statistical properties depend on. To complete the figure, also the molecular aspects involved in the definition of the individual chemical acts involved in the nucleation chemistry are of importance. Nowadays, these last aspects involve the estimation of rate constants through quantum mechanical methods.

Essentially in the past the modelling efforts were dedicated to the particle evolution while almost neglecting the reactor aspects. This was justified by the systems analyzed. Mainly, the laboratory scale reactors were simple tubular systems and they were simplified to plug flow configurations from a modelling point of view. Large industrial systems were almost not considered in the scientific literature and often simulated as well stirred reactors.

It is then clear that the industrial aerosol systems design needs a more comprehensive approach to address aspects like the nozzle design or the presence of soot collectors or preforms inside the reactor.

Modelling detailed fluid dynamics coupled with particles population balance is still a CPU expensive process. Many methodologies have been proposed for managing particle evolution equation, from discrete and sectional models[3,4] to conventional moment and quadrature of moment models[5,6]. Nevertheless, for large particle sizes and complex geometrical domains typical of industrial applications, very few methods are computationally practical.

Several researchers have dedicated works for simplifying and adapting to industrial scale the multi-scale approach. Pioneering works in the field are the following. Pratsinis at al.[7] (1986) modelled an isothermal laminar plug-flow reactor showing effects of the velocity profile on the particle concentration and size distribution. Johannessen[8] (1998) obtained by means of a commercial fluid dynamics code velocity, energy and concentration fields for an Al_2O_3 flame reactor, and then integrated over them the particle population balance equation assuming a mono-dispersed distribution. Masi et al.[9] (1999) embedded the population balance equation (PBE) in a fluid dynamics model of an un-premixed 2D turbulent jet for the production of TiO_2 particles from tetraisopropylorthotitanate ($Ti(OiPr)_4$). The full coupling, thus solving also all the complete turbulent fluid dynamics aspects through a commercial CFD code, was presented by Masi et al.[10] (2000). There, the PBE equation was rewritten through the moments of the particle distribution function. The same approach was adopted to study the nozzle configurations also for TiO_2 production from $TiCl_4$ oxidation in laminar conditions by Masi et al.[11] (2001).

Wherever possible, reactor CFD models are to be validated against production operating measurements. Nevertheless, many industrial aerosol processes are not usually suitable for *in situ* measurements and in general for on-line sampling, so that fluid dynamics models can hardly be validated by industrial data. Therefore, an effective modelling approach consists of validating the model against laboratory scale data, and then to apply it to the industrial case. An application of this technique will be described in this paper, where experimental data for different ceramic materials are used to validate the model. Thus, the simulations were differentiated by simply changing the chemical kinetics and transport data to account for the

particular system analyzed and obviously by considering the proper reactor geometry. In particular, besides the TiO_2[10,11] and ZrO_2[12] powders synthesis, the first full modelling application to the optical fibre production by an Axial Vapor Deposition (AVD) process will be presented.

2 COUPLING FLUID DYNAMICS TO PARTICLE POPULATION BALANCE

For aerosol reactors, the multi-scale approach consists of handling phenomena that involve spatial scales ranging from nanometer to meter and temporal scales ranging from fraction of second to second. Nanometer dimensions characterise primary particles, while meter refers to the geometrical dimensions of reactor; between these borders there are several other scales, such as turbulence scale, micro-particles scale, mean gas molecular path. As for temporal scales, characteristic times of coagulation, sintering and other particle phenomena may correspond to nanoseconds, while the reactor residence time is of order of seconds. Analysis of these scales and their comparison is fundamental in industrial reactor design as it identifies most significant involved phenomena and it leads to possible assumptions for saving CPU time. For instance:

- comparing mean gas molecular path to particle diameter one can define the governing particle transport regime, free or continuum,
- comparing particle diameter to turbulence scale one can neglect or not turbulence coagulation effects,
- comparing coagulation time to sintering time one can assume spherical or fractal-like particles.

The presence of two phases, solid and fluid, should be rigorously described by a multi-phase modelling approach; however, aerosols here studied are characterised by low particles concentrations, smaller than 0.1% (vol.), and by small particle Stokes numbers: in these conditions the solid phase does not alter significantly the fluid dynamics (one-way coupling). The particle evolution must be accounted for by a balance equation, the PBE, which takes into account relevant phenomena. As sketched in Figure 1, the transformation of precursors in solid particles involves both chemical and physical processes. In the systems here considered, main phenomena are limited to particle diffusion and convection, nucleation and coagulation. Other phenomena such as growth, sintering and breakage are negligible as surface reactions or gas condensation are not promoted in the investigated systems, sintering time is much longer than coagulation time and particles are hard-agglomerated. The resulting PBE for a system that has reached stationary conditions can be defined as[13]:

$$\mathbf{w}\cdot\nabla f(v) - \nabla\cdot\left(D_p\nabla f(v)\right) = N(v_0)\delta(v - v_0) + \\ + \frac{1}{2}\int_0^v \beta(v - v', v')f(v - v')f(v')dv' - f(v)\int_0^\infty \beta(v, v')f(v')dv' \quad (1)$$

where f(v) is the particle distribution function based on the volume, representing the number of particles of volume v per unit reactor volume, β(v,v') is the coagulation coefficient involving particles of volume v and v', v_0 is the monomer volume and $N(v_0)$ is the nucleation

rate that, for the systems under examination here, coincides with the solid monomer reaction of formation. The second and the third terms in the right-hand side of equation (1) are the gain and loss of particles due to coagulation, respectively. The most critical parameter to be defined is the coagulation coefficient as it depends on kind of coagulation and on the particle transport regime. However β expressions in the *free-molecule* (Kn>>1, Kn=Knudsen number) and in the *continuum* (Kn<<1) regimes can be found in the literature[4]. For intermediate regimes, an asymptotic combination of the two can be adopted[4]. The coagulation coefficient is mainly a function of the dimensions of the colliding particles and of their kinetic energy. The relationships usually refer to spherical particles, but corrections related to their fractal dimension have been proposed[14]. These corrections increase the β value because the greater cross-section of non-spherical or branched particles. In the investigated systems, particle diameter that gives Kn=1 is of order of 0.1÷0.3 μm, which corresponds approximately to the more frequent diameter of the particle distribution function. It means that in the reactor free, continuum and transition regimes can coexist.

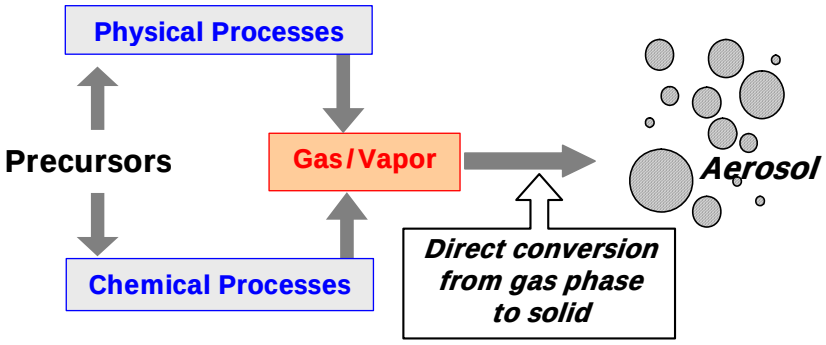

Figure 1: Steps involved in solid particle growth.

As indicated by the two terms reported in the l.h.s. of eq. (1), solid particles move by convection and by diffusion. It is important to note that, when significant temperature gradients are present like in the flame assisted systems, the particle velocity **w** is the sum of the gas velocity **u** and of the thermophoretic contribution[15] $\mathbf{w} = \mathbf{u} - 0.554\mu\nabla T / \rho T$.

Gas velocity and temperature appear in eq. (1), so it is necessary to solve the reactor fluid dynamics through continuity, momentum, energy and scalars equations[28]:

$$\nabla \cdot (\rho \mathbf{u}) = 0 \tag{2}$$

$$\rho \mathbf{u} \cdot \nabla \mathbf{u} + \nabla P = \rho \mathbf{g} + \nabla \cdot \left[\mu \left(\nabla \mathbf{u} + \nabla \mathbf{u}^T \right) - \frac{2}{3} \mu \mathbf{I} \nabla \cdot \mathbf{u} \right] \tag{3}$$

$$\rho C_p \mathbf{u} \cdot \nabla T = \nabla \cdot (\lambda \nabla T) + \sum_j R_j (-\Delta H_j) \tag{4}$$

$$\rho \mathbf{u} \cdot \nabla Y_i = -\nabla \cdot \left[\rho D_i \left(\nabla Y_i - \alpha_i^T Y_i \nabla \ln T \right) \right] + W_i \sum_j \nu_{ij} R_j \tag{5}$$

where P, μ, ρ, Cp and λ are the system pressure, viscosity, density, specific heat and thermal conductivity of gas, while Y_i, W_i, D_i, α_i^T are the mass fraction, molecular weight, mass and thermal diffusion coefficient of the ith species, respectively. Moreover, ν_{ij}, ΔH_j, R_j are the stoichiometric coefficient for ith species, the enthalpy and the rate all inherent to the jth reaction. Finally, subscript ^{T} and **I** identify the transposed matrix and the unit matrix.

Though the computational system composed by eqs. (1) to (5) allows to rigorously describe the aerosol system, it cannot practically be used as it is very CPU expensive, especially for large geometrical domains requiring a dense spatial discretisation and for systems involving complex reaction mechanism with a large number of chemical species. Accordingly, a simplified approach should be adopted. For example, the above integral-differential eq. (1) can be reduced to N simpler equations by means of the moment method[2,5]. In the following examples, only the first three moments (e.g., M_0, M_1 and M_2) and the fractional ones, easily derived from these three by assuming a unimodal lognormal distribution, were considered to keep the dimension of the problem solvable. Thus, the integral-differential PBE (1) can be approximated by the following three differential equations:

$$\mathbf{w}\cdot\nabla M_0 - D_p\nabla^2 M_0 = N - \Omega M_0^2 \tag{6}$$

$$\mathbf{w}\cdot\nabla M_1 - D_p\nabla^2 M_1 = v_0 N \tag{7}$$

$$\mathbf{w}\cdot\nabla M_2 - D_p\nabla^2 M_2 = v_0^2 N + 2\Psi M_1^2 \tag{8}$$

where Ω and Ψ represent the harmonic average on the coagulation coefficients. Equations (6) to (8) are numerically more manageable than the original PBE and require less computational resources while guaranteeing an acceptable level of approximation. Besides their statistical meaning, moments represent as well important properties: M_0 gives the particle concentration number density, $\#/m^3$, M_1 identifies the overall particle volume density, $\# m_p^3/m^3$, M_2 is related to the polydispersity of the distribution, while $M_{1.5}$ leads to the particle area density, $\# m_p^2/m^3$ (where fractional moments can be calculated by means of the first three moments only, $M_k=M_0 v_0^k \exp[9/2k^2\ln^2\sigma]$).

For the metal oxide particle synthesis, the lognormal fits with good approximation the actual shape of the particle distribution as showed by experimental results[17,18,19]. It is indeed important to remark that the assumption of locally monodispersed distribution does not force that of the collected particles to be still monodispersed[11].

The aerosol model constituted by equations (2) to (8) was defined for a laminar flow. In case of turbulence conditions, additional equations must be accounted for, depending on the chosen turbulence model. In that case, also modelling parameters such as coagulation coefficient or turbulence diffusivity should be properly defined. For instance, in the examples below, the k-ε model was adopted[16].

Finally, as our purpose is to simulate industrial scale systems, the model was introduced in commercial CFD codes because their versatility in handling complex geometrical domains and the possibility to introduce user-defined variables. In particular, CFX[20] and STAR-CD[21]

were adopted for the examples here presented, where eq. (6) to (8) were inserted by means of user Fortran subroutines.

3 METAL OXIDE PARTICLES BY VAPOR-PHASE

Chemical vapor-phase routes for nano- and micro-powders production can be characterised according to the kind of chemical reaction and its operating conditions. Main industrial aerosol applications present three different routes: fuel-oxidant driven combustions, oxidation reactions and hydrolysis reactions. The first ones lead to so-called flame reactors, where metal containing precursor and the oxidant are introduced in a chamber heated by the heat released by fuel-oxidant combustion occurring in the same chamber. Depending by the chamber geometry and by the nozzles configurations, the oxidizer can be either the oxygen introduced or the water produced by the combustion. In the other processes, the reactor is heated externally and thus only the reactions between the metal precursor and the oxidant take place. Generally, most important precursors are metal chlorides because of their high reactivity, high vapour pressure and essentially their low cost. Moreover, the chemical routes involving metal chlorides are rather simple, involving the homolytic dissociation of the Me-Cl bond as rate determining step, as verified by a quantum mechanical studies. Moreover, the reaction order with respect to the oxidant is often zero because it is fed into the reactor in large stoichiometric excess. Thus, the main overall reactions occurring in these systems are:

$$MeCl_{4\,(g)} + O_{2\,(g)} \rightarrow MeO_{2\,(s)} + 2Cl_{2\,(g)} \quad \text{(r1)}$$

$$MeCl_{4\,(g)} + 4H_2O_{\,(g)} \rightarrow Me(OH)_{4\,(s)} + 4HCl_{\,(g)} \quad \text{(r2a)}$$

$$Me(OH)_{4\,(s)} \rightarrow MeO_{2\,(s)} + 2H_2O_{\,(g)} \quad \text{(r2b)}$$

$$H_{2\,(g)} + \tfrac{1}{2}\, O_{2\,(g)} \rightarrow H_2O_{\,(g)} \quad \text{(r3)}$$

$$H_{2\,(g)} + Cl_{2\,(g)} \rightarrow 2HCl_{\,(g)} \quad \text{(r4)}$$

where Me indicates the metal and the hydrogen oxidation reaction is the most adopted flame sustaining thermally the system. The final reaction is indeed important because it helps in thermally sustain the system. Main metals following the above mechanism are Si, Ge, Ti and Zr.

The optimal process route is strongly influenced by thermodynamics[22]. Hydrolysis reaction presents a higher equilibrium constant, promoting formation of particles of a smaller size. Furthermore it is less exothermic than the oxidation, leading reactors to operate at lower temperature and allowing less expensive materials and a less important cooling section. Nevertheless, dehydroxylation reaction (r2b) can be neglected, or considered infinitely fast, as at the reaction temperature hydroxides are thermodynamically highly instable. Thus, from a modelling point of view, reactions (r2a) and (r2b) can be lumped together in $MeCl_{4(g)} + 2H_2O_{(g)} \rightarrow MeO_{2(s)} + 4HCl_{(g)}$. Rate constants for these high temperature reactions can be

estimated with reasonable approximation by the collisional theory[23] as a function of the mass and the collisional diameter of the colliding molecules. However, the today available quantum mechanical methods, like those based on the Density Functional Theory[24,25], allow reliable estimations of these rate constants. The numerical values for the most relevant thermodynamic and kinetic data for the species of interest here are summarized in Table 1.

Since MeO_2 particles are characterised by a very low vapour pressure and their monomers present a diameter larger than the Kelvin's critical diameter, the particle nucleation rate corresponds to the chemical reaction rate $N=N_{Avo}R$.

		H_2	Cl_2	$SiCl_4$	$GeCl_4$	$TiCl_4$	$ZrCl_4$
Oxidation reaction (r1), (r3)	ΔH°	-	-	-242.8	-80.0	-175.5	-227.6
	k	$2.3\cdot10^{12}$	-	$3.1\cdot10^{16}$	$8.0\cdot10^{10}$	$8.4\cdot10^{4}$	$8.4\cdot10^{4}$
	E	235.1	-	401.9	221.9	88.8	126.3
	n	1.6	-	1	1	1	1
	m	0.7	-	1	1	0	0
Hydrolysis reaction (r2)	ΔH°	-	-	-128.4	34.4	-61.1	-113.2
	k	-	-	$1.0\cdot10^{16}$	$2.6\cdot10^{10}$	$2.4\cdot10^{10}T^{0.5}$	$1.7\cdot10^{11}T^{0.5}$
	E	-	-	186.9	103.2	0	0
	n	-	-	1	1	1	1
	m	-	-	1	1	1	1
Reduction reaction (r4)	ΔH°	-		-	-	-	-
	k	-	$9.4\cdot10^{6}$	-	-	-	-
	E	-	120.4	-	-	-	-
	n	-	1	-	-	-	-
	m	-	2	-	-	-	-

Table 1: Most relevant thermodynamic and kinetic data for the systems here examined. Rates in kmol/m^3/s and concentrations in kmol/m^3. ΔH, E in kJ/mol. n, m reaction orders for the Me and the oxidant.

4 OPTICAL FIBRES CLADDING BY AVD PROCESSES

Optical fibres are characterized by the modulation of the refraction index along their radius. Particularly, a high refraction index material is surrounded by a low refraction index one. This refraction index modulation is repeated several times in a radius of a few microns.

Convenient ways to produce optical fibres are the Axial Vapor Deposition (AVD) or the Outside Vapor Deposition (OVD) processes. Their physics is the same but they differ in the shape of the chamber and in the gas injection system. There, a multi jet concentric nozzle injects the SiO_2 and GeO_2 precursors, mainly chlorides, into a diffusion flame where the oxides particles are produced. Then, those particles, driven by the gas flow, stick on a rotating target called the perform, as illustrated in Figures 2a and 2b. As a result, the flux of particles impinging on the target surface leads to a preform characterized by a very high porosity (*e.g.*, more than 95 %). Once the preform desired shape is obtained, it is then shrunk to the desired diameter of a few micron and to a length of several kilometres, by a subsequent spinning process. If the nozzle realizes a separate injection of the precursors into the flame, it is possible to produce axially modulated layers of different kind of particles sticking on the preform, thus originating on dimensions of the order of centimetres the same final structure of

the fibre. In reality, burners with five to ten different concentric nozzles are typical in the industrial applications[2]. Essentially, the philosophy behind the AVD/OVD techniques is to design the radial profile of the refraction index at the larger preform size and then to use a spinning process to obtain the desired fibre diameter.

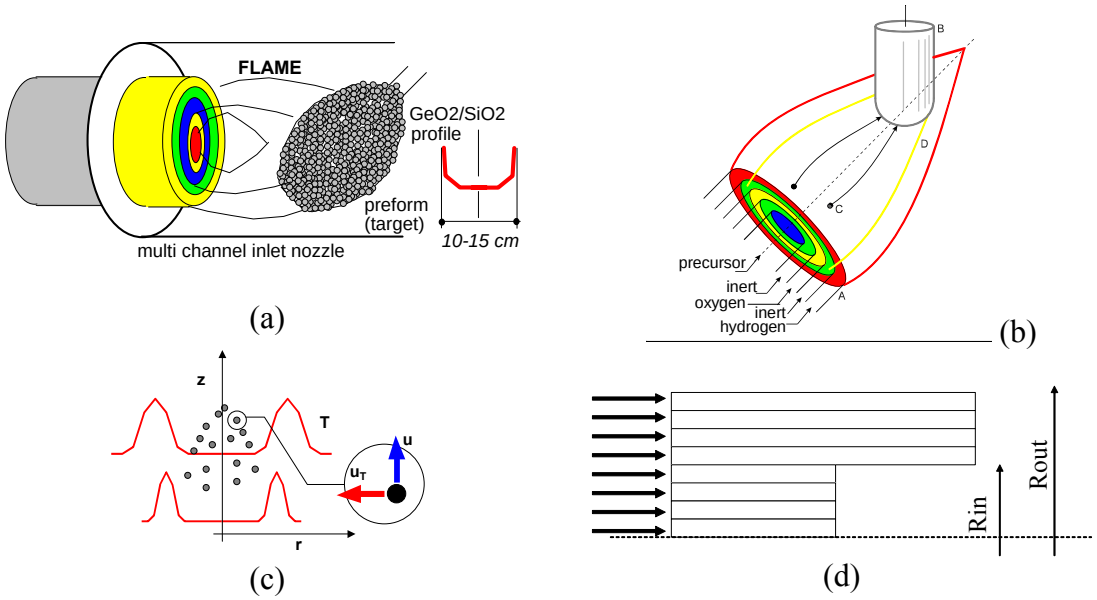

Figure 2: (a),(b) sketch of a AVD process evidencing the multi jet nozzle and the particle trajectory; (c) representation of the thermal diffusion effects induced by the flame shape on focusing the particles towards the target; (d) details of the nozzle.

An additional complication is due to engineering of the temperature profile within the flame to avoid the dispersion of the solid particles onto the reactor walls instead of their focalization on the target. This aspect is of crucial importance to obtain high yields in the deposition process. Moreover, the motion of the solid particles, nucleated in the gas phase and grown mainly by coalescence, is strongly affected by the thermoforetic forces that push the solid particles away from the hottest zone of the flame. In a traditional flame configuration, the hot zone is located along the flame axis, and thus the resulting motion of the solid particles has a significant component directed towards the reactor walls. Accordingly, to focalize the particles along the flame axis, a hot zone of annular shape has to be present in the external part of the flame, the so-called "thermal lens", illustrated in Figure 2c.

All those mentioned aspects evidence the engineering difficulties related to the proper reactor design (*i.e.*, multi-channel nozzle) and it is clear enough that to perform this job without the assistance of a model is certainly a complicated task. The example reported below is inherent to a AVD system with 8 concentric jet nozzles, alternating $SiCl_4$+Ar, H_2, Ar, O_2, Ar, H_2, Ar, O_2 and generating a flame that impacts on a almost cylindrical perform located at about 15 cm from the nozzle. The overall flow rate was 6.5 g/s and the outer diameter of the nozzle was 3 cm. The last four external nozzles were located ahead the first four, to obtain the particle generation in a confined system and then to use the external flame to focalize them

towards the target, as sketched in Figure 2d. The H_2/O_2 flame was adopted to thermally sustain the system. The simulation results are summarized in Figure 3, where the gas velocity, temperature and composition as well as the first moment and the average particle diameter fields are reported.

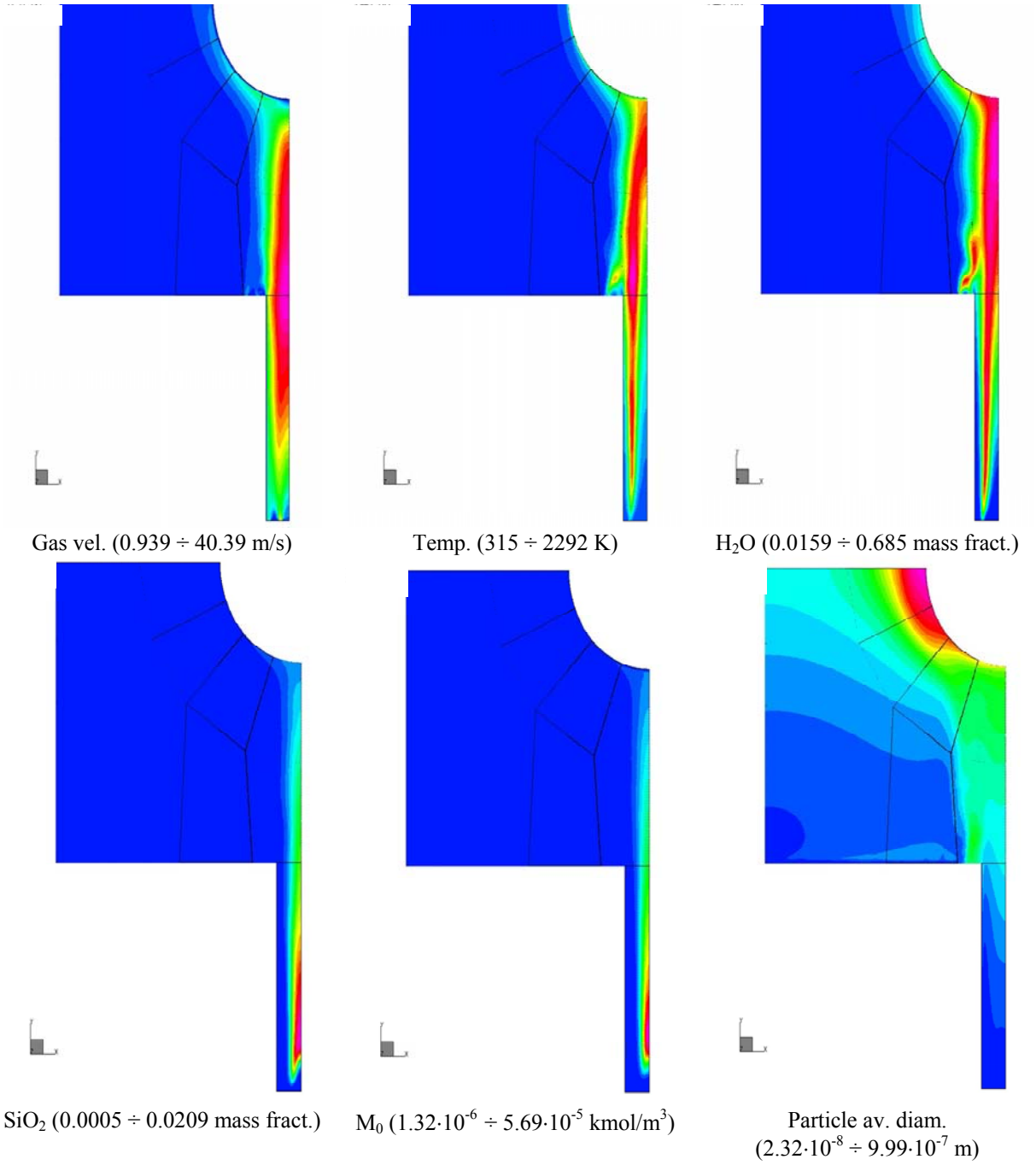

Gas vel. (0.939 ÷ 40.39 m/s)

Temp. (315 ÷ 2292 K)

H_2O (0.0159 ÷ 0.685 mass fract.)

SiO_2 (0.0005 ÷ 0.0209 mass fract.)

M_0 ($1.32 \cdot 10^{-6} \div 5.69 \cdot 10^{-5}$ kmol/m^3)

Particle av. diam. ($2.32 \cdot 10^{-8} \div 9.99 \cdot 10^{-7}$ m)

Figure 3: Calculated features of the $SiCl_4/SiO_2$ AVD process (max and min values between brackets).

By the inspection of the reported plots, it can be seen that particles nucleate near the inner nozzles inlet and their density sharply decreases because the Brownian coagulation. Their diameter increases up to about 1 μm in correspondence of the preform edge. Gas velocity and temperature reach 40 m/s and 2300 K, respectively, while the reaction occurs mainly by hydrolysis.

It is important to notice that, as more clearly evidenced by Figure 4a, the particle size increases while proceeding along the coordinate following the preform edge profile, as well as the spreading of the distribution reduces while approaching the preform. In fact, the reduction of the gas velocity approaching the tip increases the residence time in favour of the particles coagulation. More interesting is the analysis of the growth profile along the preform edge. As evidenced by Figure 4b, this profile is strongly dependent by the rate-determining step controlling the particle deposition on the preform. While a monotone behaviour is obtained in chemically controlled regime (i.e., for low sticking coefficients), the growth in transport controlled regime exhibits a maximum thus leading to a more difficult control of the preform shape. However, the preform temperature controls the shift from one to the other.

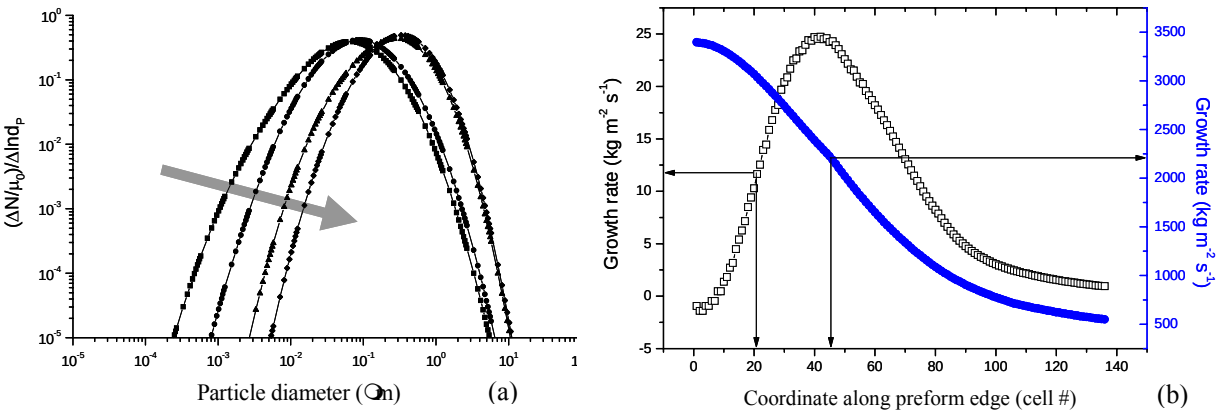

Figure 4: (a) evolution of the particle size distribution along the reactor axis while approaching the preform tip; (b), growth rate along the preform edge profile (0 = tip) under chemical (line) and diffusive (dots) regimes.

5 VAPOR-PHASE SYNTHESIS OF ZrO_2 MICRO-POWDERS

Zirconia is gaining economical importance and its cost places it as one of the most expensive products produced by an aerosol process. Accordingly, our interest was to verify our model to lately to be used for checking the performance of industrial reactors.

The scientific literature about ZrO_2 synthesis by vapour-phase route is limited to very few papers. Actually, none were available on industrial reactors and only one sufficiently describes ZrO_2 synthesis via oxidation[12] using a 30 mm in diameter, 300 mm in length cylindrical reactor, externally heated to 1000°C and presenting a concentric nozzle configuration (internal nozzle 4 mm in diameter) to separately inject the $ZrCl_4$ and O_2. Therefore, this last system was adopted for testing purposes and simulated through a two-dimensional axial-symmetric model.

In the simulation illustrated in Figure 5, the total gas flow rate was kept at 0.229 L/min at 1100°C and 1 atm with 52.5% of O_2, 0.7% of $ZrCl_4$ and balance N_2. The resulting fluid dynamics regime was laminar and the thermophoretic contribution was negligible. The comparison between the calculated and the experimental cumulative particle size distribution is illustrated in Figure 6. It can be seen that the model fit adequately with the experimental data by using parameters fully taken from the literature and thus without any adjustments on the examined system.

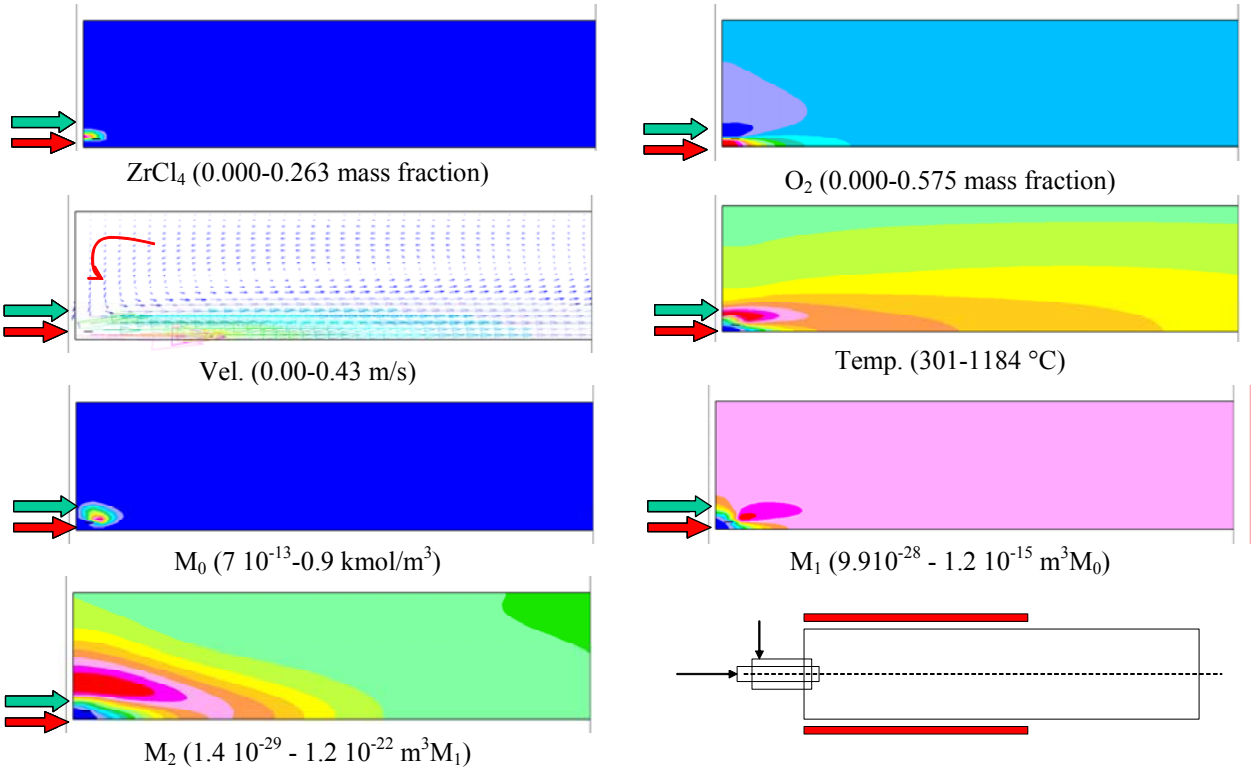

Figure 5: Calculated features of the $ZrCl_4/O_2/ZrO_2$ aerosol process. Conditions as in ref. 12, (max and min values between brackets). Last picture, r.h.s.: sketch of the experimental reactor.

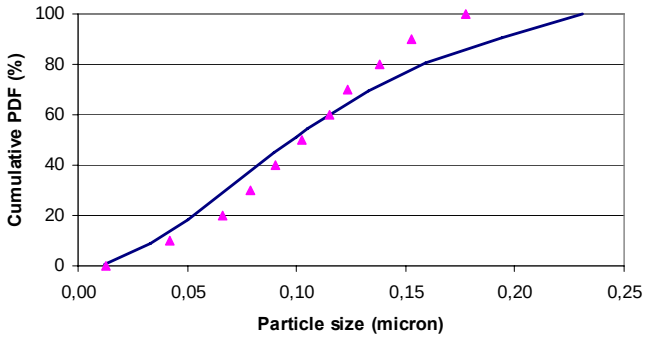

Figure 6: Comparison between modelled (line) and experimental (symbols) PDF for ZrO_2 synthesis.

6. LABORATORY SCALE TIO_2 REACTOR

To present another verification of the model capability, a laboratory scale aerosol reactor for TiO_2 particle synthesis using $TiCl_4$, O_2 and H_2O as reactant was simulated. This tubular reactor, 3.2 cm in diameter, has separate inlets for the reactants and is subdivided in four sections (pre-heating: 400 K x 14 cm, furnace: 1473 K x 26 cm, cooling to 700 K in 16 cm and exhaust: 700 K x 93 cm). $TiCl_4$ is injected in the outer channel, while H_2O/O_2 enter the reactor through the inner nozzle[17,26]. Particles were collected after the cooling section and the diameter distribution function was then obtained through an automated image analyzer.

The TiO_2 synthesis can proceed through both the oxidation and the hydrolysis reactions. Several works[18,26,27] have studied the influence of the water steam in a high-temperature flame: the presence of water during the synthesis of oxide particles introduces significant modification in the morphology and size of the particulate. Accordingly, an important challenge in this area is the understanding of which operating process parameters can be manipulated (*i.e.*, water/precursor molar ratio, inlet points, temperature, residence time…) in order to better control the final characteristics of the products. In the following, a full simulation performed for a feed molar ratio $R=H_2O/TiCl_4=0.06$ in great O_2 excess will be presented. The results of this simulation are summarized in Figure 7.

By the inspection of the reported data it can be seen that the maximum in gas velocity is located in correspondence of the H_2O inlet nozzle. The gas velocity in the outer nozzle sharply increases when the gas reaches the heated section. Finally, the velocity profile becomes almost parabolic in correspondence of the reactor exit. The temperature behaviour matches the above trends. The axial temperature gradients are maximum in correspondence of the boundaries of the heated region, while the radial ones are significantly lower. The consumption of $TiCl_4$ appears to be strongly temperature dependent. At the lower temperatures near the inlet (e.g., 400 K), the mole concentration remains substantially equal to the inlet one. Instead, when the temperature increases, the reaction takes place and in $TiCl_4$ is totally consumed in a narrow zone close to the internal nozzle.

In this case, its total consumption is reached inside the furnace and not in the preheating zone. Because its high reactivity, water is consumed almost immediately and thus its concentration is almost zero throughout all the reactor besides a narrow zone around the inlet. The M_0 evolution shows two different zones where the nucleation of particle and the initial coagulation occurs. The former is placed in correspondence of $TiCl_4$ disappearance (i.e., oxidation), while the latter is in proximity of the internal channel where H_2O enters into the reactor. The M_1 moment remains substantially constant along the reactor: the particles are nucleated almost immediately and they redistribute over the total volume by rearranging themselves by the effect of coagulation. More interesting is the resulting behaviour of the average particle diameter whose maximum values are located near the outer reactor wall: the addition of water nucleates new particle of small diameter thus reducing the average value. In any case, at any radius, the diameter increases along the reactor. Thus in this configuration the nucleation occurs mainly by oxidation.

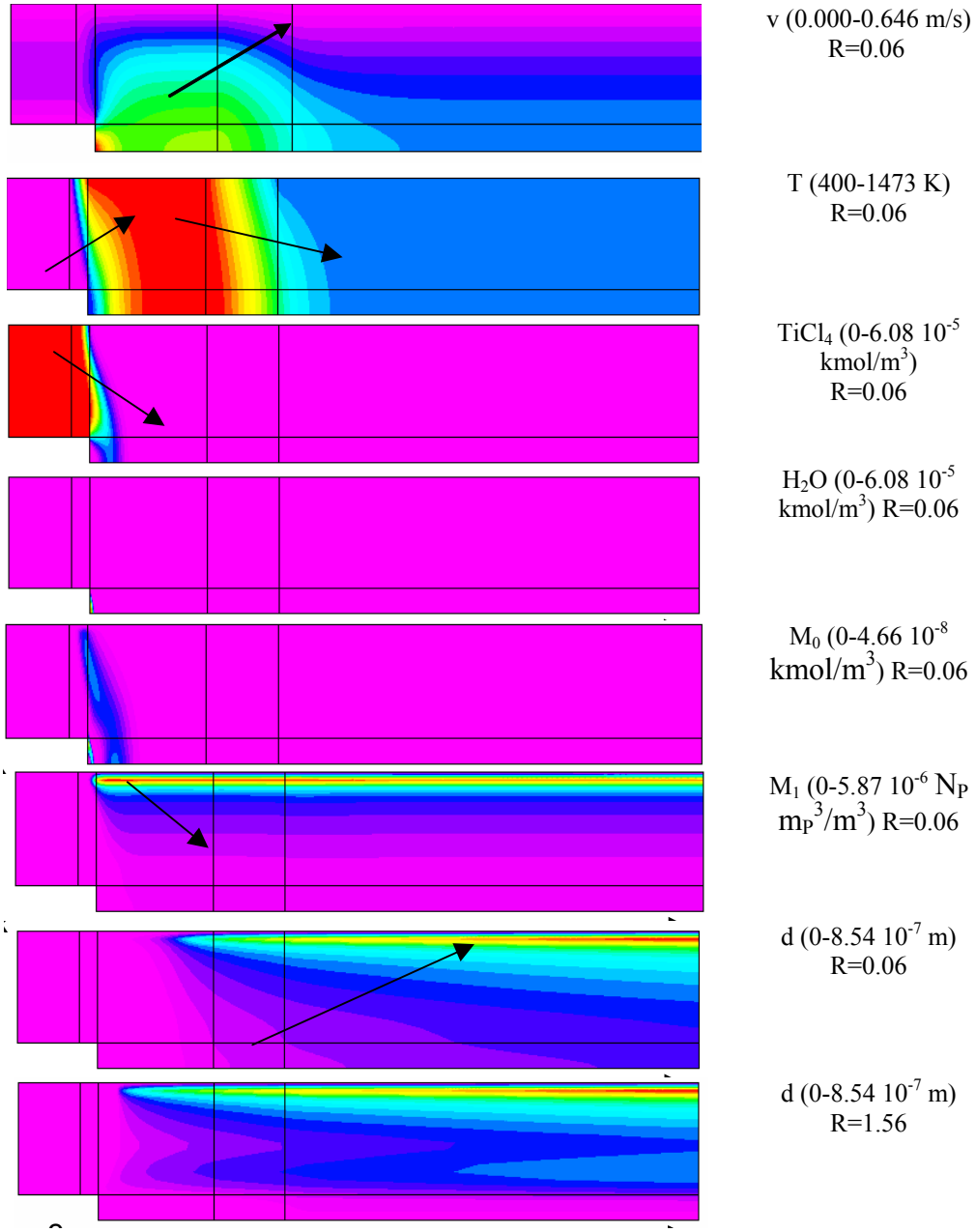

Figure 7: Calculated profiles of the axial velocity, gas temperature, $TiCl_4$ and H_2O concentrations, zeroth and first order moments of the distribution for R = 0.06 and furnace residence time 1.2s. Last row, average particle diameter for R=0.06 and R=1.56.

Repeating the simulations for different ratios of increased value obviously also the importance of the hydrolysis reaction increases.

Finally, it is important to compare the calculated averaged distribution at reactor outlet with the experimental one. This comparison is illustrated in Figure 8, showing a great

agreement between the two sets of data. Here different process conditions have been summarized, ranging from the absence of water (i.e., R=0) up to R=1.56, evidencing that the influence of the water becomes appreciable only for high R values leading to final bimodal distribution function. Analogous size distributions can be obtained also by shaping differently the inlet nozzles also by using only oxygen. Accordingly, the reactor can be designed to obtain the desired particle size distribution function.

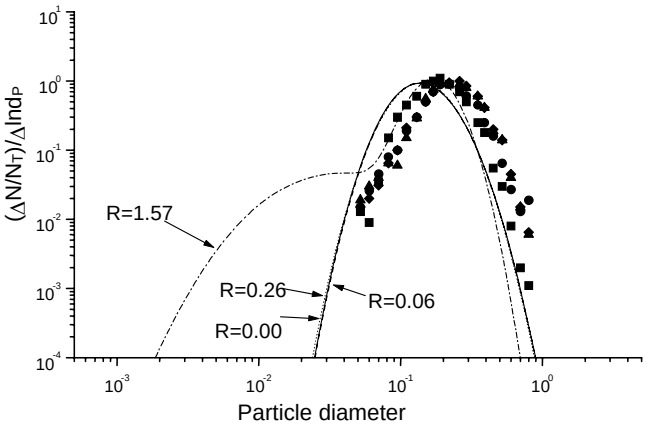

Figure 8: Comparison between experimental and calculated distribution functions for different $H_2O/TiCl_4$ molar ratio (after ref. 11).

7. INDUSTRIAL SCALE TiO_2 REACTOR

After verification of the model reliability in predicting the performance of a laboratory scale reactor, the attention was shifted to the analysis of an industrial TiO_2 reactor (length to diameter ratio of 2.25). It presents a complex geometry because the nozzle configuration is not concentric: the two reactants (i.e., $TiCl_4$+Ar and H_2O) are injected separately by two jets (reactor diameter to nozzle diameter ratio of 30) placed on the reactor half plane and oriented towards the reactor axis. This configuration leads to a large 3D geometrical domain.

The synthesis is obtained via hydrolysis reaction, at 1 atm, as it promotes particles of smaller size and temperature reaction is kept low. Water steam is fed in superheated conditions, with a nozzle tip velocity of 10.5 m/s. $TiCl_4$, carried by Ar, is fed at 500°C, with a nozzle tip velocity of 0.2 m/s. Fluid dynamic field at the outlet of the nozzles is characterised by a low-Reynolds turbulent regime (Re ≅ 10000). Nevertheless, the particle coagulation process is not significantly influenced by turbulence because its scale is greater than the particle size (scale ratio ≅ 10). Furthermore, as reactor walls are kept at the constant temperature of 500°C, which is almost the same temperature of the bulk, no significant deposition or thermophoretic effects are present.

Calculated steady state velocity, concentration and temperature fields for the above conditions are shown in Figure 9. It can be seen that key fluid dynamics phenomena (i.e., turbulence and chemical reaction) and the highest gradients are all located near the nozzles. To account for these points, a dense spatial discretisation was then applied. Because of the

injection system, reactants diffusion resulted the rate-determining step for the particle nucleation. Maximum temperature was 632 °C.

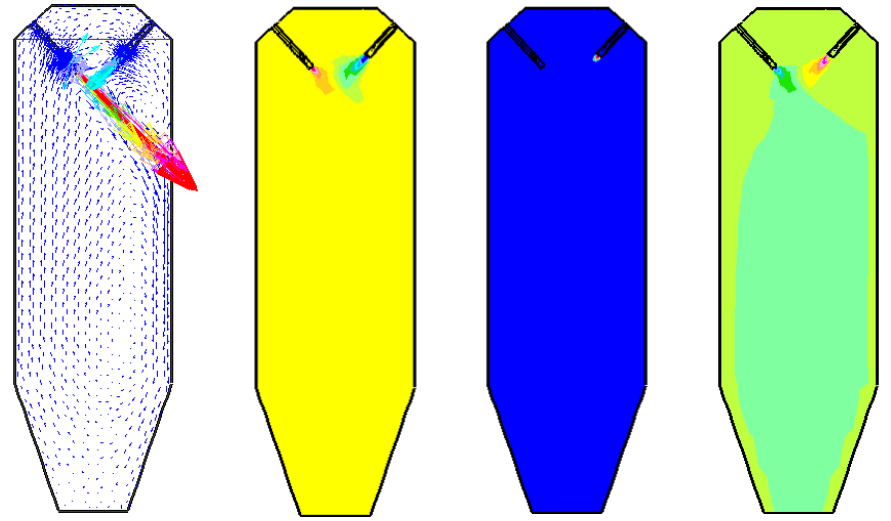

Figure 9: Velocity, concentration and temperature fields for the industrial TiO_2 reactor (max and min values between brackets).

The calculated first three moments are reported in Figure 10. Again, maximum particle concentration (M_0) and aerosol volume (M_1) were located where nucleation takes place that is in the proximity of the $TiCl_4$ nozzle. Even polydispersity (M_2) is larger around the same nozzle because the high temperature and the entrainment of the surrounding gas promote the coagulation process among particles of different sizes. The uniform distribution of statistical moments in the remaining volume of the reactor indicates that there is an effective gas re-circulation, as showed by the velocity field. Pictures evidence also that particle evolution phenomena are mainly positioned near the nozzles.

Finally, the comparison between calculated and experimental particle size distribution is reported in Figure 11. The experimental particle size distribution for production lots was obtained by means of a sedimentation apparatus that presents a maximum resolution limit at 0.15 μm. Nevertheless, the resolution of the instrument is enough to highlight the lognormal shape of the distribution.

Also for this case, it can be seen that model described in section 2 fits adequately with the experimental data by using parameters fully taken from the literature and thus without any adjustments on the examined system. It is then clear that parameters estimated on small-scale systems when introduced in a rigorous modelling framework are able to well reproduce even large scale industrial systems.

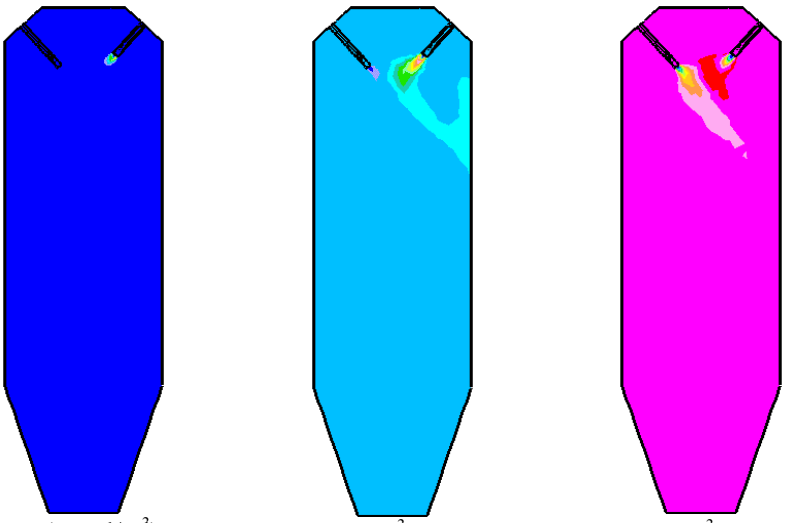

Figure 10: Calculated statistical moments, order one, two and three (max and min values between brackets).

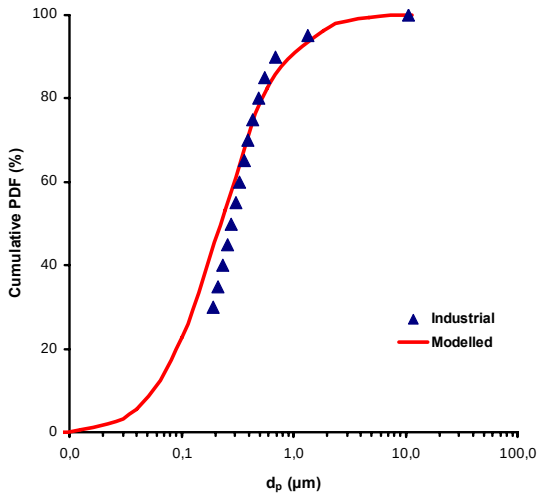

Figure 11: Comparison between modelled (line) and industrial (symbols) cumulative PDF for TiO_2.

8. CONCLUSIONS

In this paper a general framework modelling approach for industrial aerosol reactors for metal oxide particle production was described. Fluid dynamics and particle population balance equations were fully coupled in commercial CFD codes and then tested against three important aerosol systems.

Particularly, the optical fibres production through AVD processes, the ZrO_2 synthesis via $ZrCl_4$ oxidation and the TiO_2 synthesis via oxidation/hydrolysis were examined. In both cases, no direct experimental monitoring of the system is available and thus, the model offers new important insights in understanding the complex phenomena involved in the process. In both cases, the use of parameters taken from the literature or estimated on small scale systems allows the quantitative prediction of the process performance and features at industrial scales without the necessity of parameters tuning. This point remarks the importance of the chemical engineering approach in all the scale-ups involved in the manufacturing industry.

REFERENCES

[1] W.C. Hinds, *Aerosol technology*, Wiley, New York (1982).

[2] T.T. Kodas, M. Hampden-Smith, *Aerosol processing of materials*, Wiley, New York (1999).

[3] F. Gelbart et al., "Sectional representations for simulating aerosol dynamics ", *J. Colloid Interface Sci.*,68 (1980).

[4] J.D. Landgrebe, S.E. Pratsinis, "Gas phase manufacture of particulates: the interplay of chemical reaction and aerosol coagulation in the free molecular regime", *Ind. Eng. Chem. Res.*,28,1474-81 (1989).

[5] S.E. Pratsinis, "Simultaneous nucleation, condensation and coagulation in aerosol reactors", *J. Colloid Interface Sci.*, 124,416-427 (1988)

[6] R. McGraw, "Description of aerosol dynamics by the quadrature method of moments", *Aerosol Sci. Technol.*,27,255-265 (1997).

[7] S.E. Pratsinis et al., "Aerosol reactor design: effect of reactor type and process parameters on product aerosol characteristics", *Ind. Eng. Chem. Process Des. Dev.*, 25,634-642 (1986)

[8] T. Johannessen et al., "Computational fluid particle dynamics of flame synthesis of alumina particles by coagulation and sintering", *Chem. Eng. Sci.*, 55, 177-191 (2000).

[9] M. Masi et al., "Modelling of aerosol reactor for synthesis of TiO_2 powder", ICheaP-4, AIDIC Milano, 616-618 (1999)

[10] M. Masi et al., "Modelling of aerosol deposition of titania thin films", *Materials Chemistry and Physics*, 66,286-293 (2000)

[11] M. Masi et al., "CFD modelling of aerosol reactors for materials synthesis", *Electrochemical Soc. Symp. Ser.*, 13, 488-495 (2001)

[12] Y. Suyama et al., "ZrO_2 powders produced by vapour phase reaction, *Ceramurgia International*, 3, 141-146 (1977)

[13] S.K. Friedlander, *Smoke, Dust and Haze: fundamentals of aerosol behaviour*, Wiley (1977)

[14] S.N. Rogak et al., "The mobility and structure of aerosol agglomerates", *Aerosol Sci. Technol.*, 18(1),25-47 (1993)

[15] G.M. Homsy et al., "Blasius series for thermophoretic deposition of small particles", *J. Colloid Interface Sci.*, 83 (1981)

[16] J.O. Hinze, *Turbulence*, McGraw-Hill Book Company, 2nd ed. (1975)

[17] M.K. Akhtar et al., "Vapor synthesis of titania powder by $TiCl_4$ oxidation", *AIChE J.*, 37**,** 1561-1570 (1991)
[18] S.E. Pratisinis, P.T. Spicer, "Competition between gas phase and surface oxidation of $TiCl_4$ during synthesis of TiO_2 powder", Chem. Eng. Sci., 53 (1998)
[19] S.M. Suh et al., "Numerical modelling of SiO_2 particle formation and transport in a one-dimensional low-pressure chemical vapour deposition reactor", *J. Aerosol Sci.*, 33, 943-959 (2002)
[20] CFX-4 by ANSYS, Inc.
[21] STAR-CD by CD-adapco
[22] O. Knacke et al., *Thermochemical properties of inorganic substances*, 2nd ed., Springer-Verlag, Berlin (1991)
[23] S.W. Benson, *Thermodynamical kinetics*, Wiley, New York (1976)
[24] H. Simka, et al., "Computational chemistry predictions of reaction processes in organometallic chemistry", *Progr. Crystal Growth Character. Mater.*, 35, 117-149 (1997)
[25] C. Cavallotti, et al., "Accelerated decomposition of gas phase metal organic molecules determined by radical reactions", *J. Crystal Growth*, 266, 363-370 (2004)
[26] M.K. Aktar et al., "Competition between $TiCl_4$ hydrolysis and oxidation and its effect on product TiO_2 powder",*AIChE J.*, 40**,** 1183-1192 (1994)
[27] H. D. Jang, "Effect of H_2O on the particle size in the vapor-phase synthesis of TiO_2",*AIChE J.*, 43**,** 2704-2709 (1997)
[28] R. B. Bird et al., *Transport Phenomena*, 2^{nd} ed., J. Wiley and Sons, New York (2002)